Crossing the Thauer limit: Rewiring Cyanobacterial Metabolism to Maximize Fermentative H2 Production

SCHOLARONE™
Manuscripts

Crossing the Thauer limit: Rewiring Cyanobacterial Metabolism to Maximize Fermentative H$_2$ Production

G. Kenchappa Kumaraswamy[1], Anagha Krishnan[1‡], Gennady Ananyev[1], Shuyi Zhang[2†], Donald A. Bryant[2,3] and G. Charles Dismukes[1]*

1. Waksman Institute and Department of Chemistry & Chemical Biology, Rutgers University, Piscataway, NJ 08854, USA. *E-mail: dismukes@rutgers.edu;
    Fax: +1 848 445-5735; Tel: +1 848 445-6786
2. Department of Biochemistry and Molecular Biology, The Pennsylvania State University, University Park, PA 16802, USA
3. Department of Chemistry and Biochemistry, Montana State University, Bozeman, MT 59717, USA.

‡Present address: Department of Biochemistry, University of Alberta, Edmonton, Alberta, T6G2RE, Canada

†Present address: Department of Biological Engineering, Synthetic Biology Center, 500 Technology Square NE47-140, Massachusetts Institute of Technology, Cambridge, MA 02139, USA

Abstract

Many cyanobacteria power metabolism during dark anaerobic conditions by the catabolism of glycogen which creates adenylate energy (ATP) and NAD(P)H. The latter can be reoxidized by a reversible NiFe-hydrogenase functioning as a terminal oxidoreductase generating H_2 as byproduct. Theoretically, one glucose molecule can yield up to 12 molecules of H_2, although this never happens *in vivo*. The thermodynamic preference is for glucose catabolism via the Embden-Meyerhof-Parnas (EMP) pathway (henceforth, glycolysis) which restricts the pathway yield below 4 mole H_2/mole glucose (so-called Thauer limit). An alternate route that is not used is the oxidative pentose phosphate shunt (OPP), which theoretically can yield 3-fold more NAD(P)H than glycolysis. Herein, we engineer the cyanobacterium *Synechococcus sp. PCC* 7002 to redirect glycogen catabolic flux through OPP by deleting the *gap1* gene for glyceraldehyde-3-phosphate dehydrogenase (GAPDH-1) and stack this with a knock-out mutation of NADH-consuming lactate dehydrogenase (*ldhA*). The resulting $\Delta gap1\Delta ldhA$ double mutant when combined with the elimination of H_2 uptake by continuous electrochemical removal of H_2 was able to produce 681 µmol H_2/g DW/day, equivalent to 6.4 mole H_2/mole glucose, well beyond the Thauer limit. This achieves the highest *in vivo* autofermentative H_2 production yield of any bacterium, equivalent to 80% of the theoretical maximum of 8 H_2/glucose via OPP, using only photoautotrophically generated glycogen as precursor with full retention of cellular viability. These findings demonstrate the plasticity of central carbon metabolism and the significant potential of metabolic engineering for redirecting carbohydrate catabolism towards hydrogen production in cyanobacteria.

Introduction

As there are no natural hydrogen (H_2) deposits, and millions of tons are consumed industrially each year, its production plays a major role in all industrialized societies. The global H_2 generation market accounted for $103.20 billion USD in 2017 and is expected to reach $207.48 billion by 2026 [1], with major applications in on-site oil refining, and in the production of ammonia (Haber process) and methanol (from carbon monoxide). Steam-methane reforming - the major production process used to produce H_2 from natural gas -uses high-pressure (3-25 bar) and high-temperature (700°C–1,000°C) steam and accounts for 8.1 tons CO_2 byproduct [2] which is emitted to the atmosphere per ton of H_2. This accounts for 1.1 % of all CO_2 emissions in the US [3]. By contrast, anaerobic bioconversion of biomass to H_2 is one of the renewable options [4]. Among the various microorganisms, cyanobacteria are of special interest as metabolic cell factories for H_2 production because of their ability to produce their own carbohydrates by photosynthesis, at 1-3% conversion efficiencies at best. These carbohydrates can then be converted to H_2 using endogenous fermentative metabolism under dark anoxic conditions (autofermentation) without sacrificing the organism [5]. Many cyanobacteria are capable of both oxidizing and producing H_2 using an endogenous bidirectional NiFe-hydrogenase [6] with either NAD(P)H, flavodoxin or ferredoxin as electron carriers; however, yields are low (1-2 H_2/glucose) and rates slow when not using thermodynamic "milking" by removal of H_2 [7, 8, 9, 10, 11]. Even optimally engineered *E coli* strains can produce low levels of H_2 from supplied glucose (1.2 to 2.11 mol H_2/mol glucose) [12].

The maximum theoretical yield of H_2 from glucose is 12 moles and is accompanied by the production of 6 moles of CO_2. Combining the 11 enzymes of the oxidative pentose phosphate pathway (OPP) with hydrogenase in a cell-free system, Woodward and coworkers [13] demonstrated yields of upto 11.6 mol H_2/mol glucose. However, this complete conversion is not realized in bacteria because the oxidative pentose phosphate (OPP) pathway is not used exclusively *in vivo*. In cyanobacteria, the Embden-Meyerhoff-Parnas (EMP) pathway (henceforth referred to as glycolysis) and the OPP pathway are the two catabolic routes that can produce NAD(P)H during autofermentation. Further, if the oxidative-tricarboxylic acid cycle (TCA) can be harnessed under anaerobic conditions, the available carbon substrates can be completely oxidized to produce 12 mols of NAD(P)H. If all the NAD(P)H generated from glucose catabolism is available to NiFe-hydrogenase, then glycolysis leading to acetyl-CoA can yield 4 mol of H_2/glucose (called the Thauer limit [14, 5]), the OPP pathway can yield 8 mol of H_2/glucose (Figure 1a) and with an intact

32   oxidative-TCA cycle would yield 12 mol of H_2/glucose. However, much less than this theoretical

33   limit is made *in vivo* because: a) glycolysis is the dominant glucose catabolic route in cyanobacteria

34   under fermentative conditions as it produces more ATP, b) TCA cycle if operational under

35   fermentative conditions runs in the redox neutral-branched version and c) generating H_2 from

36   NAD(P)H is thermodynamically unfavorable under standard conditions; therefore, the reductant

37   is reoxidized by alternate fermentative enzymes rather than hydrogenase [9], [15]. In the euryhaline

38   cyanobacterium, *Synechococcus* sp. PCC 7002 (hereafter *Synechococcus* 7002) used in this study,

39   NAD(P)H is mainly reoxidized via lactate dehydrogenase (*ldhA*) making it the main competitor

40   for hydrogenase [16]. Elimination of LdhA alone in *Synechococcus* 7002 resulted in a 12% yield

41   which was 5-fold higher than that of the wild-type strain [16].

42   Besides *ldh*A deletion, other metabolic engineering strategies to overcome these

43   intrinsically low yields of fermentative H_2 production have been attempted in cyanobacteria

44   (reviewed in [17], [18], [19], [5]). These include: a) inactivation of the *narB* and *nirA* genes associated with

45   nitrate assimilation to eliminate the competition for NAD(P)H and increase H_2 yields in

46   *Synechocystis sp.* strain PCC6803 and *Synechococcus* 7002 [20], [21]; b) overcoming the kinetic

47   bottleneck in glycolysis[22] at NAD^+-dependent glyceraldehyde 3-phosphate dehydrogenase

48   (GAPDH-1) by overexpression of *gap1* [23]; and c) construction of a *gap1* null mutant *(∆gap1)* to

49   shift glucose catabolism from upper glycolysis into the OPP pathway [23]. The results with *gap1*

50   mutations were quite promising. The engineered strain of cyanobacterium *Synechococcus* 7002

51   produced significantly more H_2 whether *gap1* was inactivated or overexpressed [23], albeit for

52   different reasons. The knockout mutant genetically blocked flux through upper glycolysis and

53   yielded 5.7-fold increased intracellular NADPH and a 2.3-fold increased H_2 yield. The strain

54   overexpressing the *gap1* gene (*gap1*[OEx]) accumulated 17 % more glycogen during the

55   photosynthetic stage of growth, and subsequently produced a faster anaerobic catabolic rate,

56   yielding 4-fold larger intracellular NADH and 3-fold higher flux into H_2 production. Still, the H_2

57   yields fell well below the Thauer limit (1.1-1.4 mol H_2/ glucose without H_2 milking).

58   An alternate method to overcome the thermodynamic unfavourability of the H_2 evolution

59   reaction is to shift the equilibrium towards H_2 production by continuous removal of H_2. This can

60   be achieved using a membrane-covered electrochemical cell that selectively consumes H_2. This

61   method of "electrochemical milking" successfully accelerates the autofermentation rate and

62   increases the H_2 yield [24]. Demonstrating the thermodynamic linkage to pyruvate catabolism, the

63   uptake of H_2 (metabolic oxidation) was shown to be linked quantitatively to the production of more

64   reduced carbon products (lactic acid, acetate and ethanol). Using the fast growing cyanobacterium,

65   *Arthrospira maxima,* the fermentative yield increased to 4.68 mols H_2/mol glucose under milking

66   conditions, while catabolizing 97% of the glycogen fraction in this cyanobacterium [24], [25]. This is

67   the highest reported conversion yield yet achieved by autofermentation.

68   In the present study, we have engineered the OPP and glycolysis pathways in

69   *Synechococcus* 7002 to enhance the NAD(P)H availability for the endogenous NiFe-hydrogenase

70   and combined it with electrochemical H_2 milking to shift the equilibrium away from H_2 uptake.

71   *Synechococcus* 7002 was genetically engineered by targeting the *gap1* and *ldhA* genes, creating

72   double mutants for both overproduction and deletion of GAPDH-1 activity. A special

73   electrochemical cell was used to allow continuous removal of H_2 by electrochemical oxidation,

74   thereby converting the bidirectional NiFe-hydrogenase to a unidirectional enzyme (Figure 1b). We

75   have characterized the influence of these mutations, along with the single *ldhA* mutant and the WT

76   strains, on the metabolite pools sizes, pyridine nucleotide levels, redox balance, adenylate energy

77   charge, and the fluxes of glycogen and H_2.

78

79   **Experimental section**

80   **Strains and culture conditions.** All strains were grown photoautotrophically in A^+ medium

81   (Stevens, 1973), supplemented with 2 μM $NiCl_2$ and were bubbled with 2% (vol/vol) CO_2 in air.

82   Antibiotics, spectinomycin (50 μg ml^{-1}), kanamycin (100 μg ml^{-1}), gentamycin (20 μg ml^{-1}) and

83   erythromycin (20 μg ml^{-1}) were added wherever required. Cells were grown to densities of

84   approximately 10^8 cells mL^{-1} at 38 $^\circ$C with a light intensity of 200 μmol photons m^{-2} s^{-1}. The

85   strains were then switched to dark anoxic conditions to induce fermentative metabolism. For

86   growth rates, cells were grown in A^+ medium, under an irradiance of 200 μmol photons m^{-2} s^{-}

87   ^{1}with constant bubbling of 2% CO_2 in air. Growth data were fitted to a Gompertz function [26] to

88   calculate the specific growth rates.

89

90   **Strain construction.** To generate the mutant strains, GAPDH-1 (*SYNPCC7002_A2697*)

91   overexpression strain *(gap1^{OEx})* and Δ*gap1* deletion strains and the *ldhA* mutant described and

92   characterized previously [23], [16] were the base strains (Table 1). Genomic DNA of Δ*ldhA* was used

93   to amplify the *ldhA::aacC1* fragment by PCR using the primers, Ldha1F (5′

94   AATACATTGCCCTACGCTGTGC 3′) and Ldha1R (5′ GGTCAACTTTTGCTTCCTTTCGG 3′)

95   (Figure S1). The resulting amplicon was used to transform the *gap1^OEx* and Δ*gap1* strains to delete

96   *ldhA* via homologous recombination as described in [27]. Gentamicin resistance was used as the

97   selection antibiotic [27]. Complete segregation of *ldhA* and Δ*ldhA::aacC1* alleles in the resulting

98   *gap1^OEx*Δ*ldhA* and Δ*gap1*Δ*ldhA* strains was verified by PCR (Supplementary Figure S1).

99   **Autofermentation.** Upon reaching late exponential phase at an OD_{730} of 1.2, cultures (100 ml

100   volume) were harvested by centrifugation, washed once with nitrate-free medium A and

101   resuspended in 100 mL of nitrate-free medium A. Aliquots (5 ml) were placed in glass vials (10-

102   or 20-mL and sealed with a crimp-top Teflon lined rubber stopper. Vials were wrapped with

103   aluminum foil to create dark conditions.The headspace of all the vials was purged for 20 min with

104   argon gas to create anoxic conditions. Four replicates were prepared for each strain for each time

105   point. A conversion coefficient of 0.99 mg DW/10^8 cells was used for normalizing the data to dry

106   weight.

107

108   **Extracelluar metabolite analysis.** For H_2 measurement, the headspace gas was measured using

109   gas chromatography (GC) at each timepoint after induction of fermentation. Headspace gas (200

110   µL) was sampled using a gas-tight syringe and analysed with a Perkin Elmer Clarus 680 gas

111   chromatograph equiped with a thermal conductivity detector with argon as the carrier gas [28]. For

112   each timepoint measurement, four replicates were sampled and their mean values and standard

113   deviations were used for statistical comparisons.

114

115   **Intracellular reduced carbohydrate analysis.** The anthrone-sulfuric acid method was used to

116   determine the total reduced carbohydrate content in the cells [29].

117

118   **Metabolomics of fermenting cells (LC-QQQ-MS).** Intracellular metabolite analysis was done

119   by extracting and analysing the metabolites from the cells as previously described [30]. Briefly, the

120   cells (2 mL) from the fermentation vials were sampled using a syringe and were immediately

121   vacuum-filtered onto a 0.45-µm membrane filter under dark conditions. The membrane filters were

122   quickly inverted into 80:20 MeOH/H_2O (1.8 mL, precooled to –20 °C) in clean Petri dishes,

123   followed by a 20-min incubation at –20 °C. After incubation, the cell material was scraped off the

124   membrane filters and the solvent with the cells was transferred to microfuge tubes. The solvent

125   was centrifuged at 14,000 × *g* at 4°C for 5 min, and the supernatant was removed and stored at −

126   20 °C. The solvent (120 μL) was vaccum-dried (Labconco Centri-Vap Concentrator), and the

127   pellet was resuspended in LC-MS grade water (20 μL) and transferred to LC-MS vials for analysis.

128   The metabolites were analysed by injecting an aliquot (10 μl) of the sample into an Agilent 1200

129   series HPLC coupled to a 6490 QQQ mass analyzer equipped with an ion-spray source (Agilent

130   Technologies, Waldbronn, Germany). The samples were separated using a XRs 3 C18 column (50

131   × 2.0 mm, Agilent Technologies) with gradients of 11 mM acetic acid + 10 mM tributylamine in

132   water as solvent-A and methanol as solvent-B with a flow rate of 0.33 mL min^{-1}. The MS was

133   operated in negative ionization mode and the data acquired was analysed using Agilent Mass

134   Hunter software (Build 1.04).

135

136   **"H$_2$ milking".** Electrochemical consumption of H$_2$ from the fermenting cell culture was

137   performed using a home-built electrochemical cell based on "fuel cell technology" [24]. A 4 mm

138   polarized Pt–Ir electrode covered with a thin 5-μm Teflon membrane in contact with culture

139   volume (8 μL) served to oxidize H$_2$ [31]. The H$_2$ rate is measured as electrical current (I, nA) that

140   was converted to gas moles using Faraday's second law [32] after digital integration for the 20 h of

141   fermentation (total electrical charge dQ = I × dt (Coulomb)). Upon normalization to the total

142   number of cells loaded onto the electrode and using the conversion coefficient of 0.99 mg DW/10^8

143   cells, nmoles of the H$_2$ produced was converted to nmoles/mg DW.

144

145   **Pyridine Nucleotides.** NAD$^+$, NADP$^+$, NADPH and NADH levels were determined in two ways.

146   LC-MS/MS was used to measure extracellular oxidized and reduced forms of each following

147   extraction [23]. For simultaneous measurement of NAD(P)H along with H$_2$ rate, the sample from the

148   top at a 45^0 angle were illuminated by pulsed illumination (250 ms) using UV-365 nm LED

149   (Nichia, Japan) built in the Pt-Ir electrode. This source (optical power 1000 W/cm^2) was pulsed at

150   a fixed duty cycle of 20% (0.2 s on, 0.8 s off). This illumination has been found to have a negligible

151   effect on photosynthetic electron transfer and autofermentative dark H$_2$ production. The 450 ± 30

152   nm interference filter (Intor, Inc., US) was used to select NAD(P)H fluorescence emission. Further,

153   the signal from an amplified photodiode S5591 (Hamamatsu Photonics, Japan) was filtered by a

154   preamplifier in the range of DC-100 Hz (Model 113, EG&G, US). Please refer to [24] for complete

155   details for the set up and usage of this electrode.

156   **Results**

157   **Mutant construction and growth physiology**

158   The metabolic modifications were chosen to increase intracellular reductant production during

159   dark anoxic condition and to eliminate a competing reductant sink, pyruvate → lactate. Two

160   mutant strains were constructed: a) a strain in which both the *gap1* and *ldhA* genes were deleted

161   *(Δgap1ΔldhA)*, and b) a strain in which the *gap1* gene was overexpressed (*gap1^{OEx}*) (GAPDH-1)

162   combined with the deletion of *ldhA* (*gap1^{OEx}ΔldhA)* (see Experimental section, Table 1).

163

164   Photoautotrophic growth of *Δgap1ΔldhA, ΔldhA*, *gap1^{OEx}ΔldhA* and WT strains was studied under

165   constant illumination of 200 µmol photons m^{-2} s^{-1} with CO_2 sparging. All the strains had similar

166   growth rates (Table 2; Figure S2).

167

168   **Hydrogen production under fixed headspace.**

169   H_2 production in the strains under dark anoxic conditions was monitored daily over 4 d. Cells were

170   incubated in sealed vials with a fixed argon filled headspace volume of either 5 or 15 mL. Figure

171   2a gives the headspace H_2 content on each day in the 5-ml vials. Compared to WT after 4 d, the

172   *Δgap1ΔldhA* and *ΔldhA* strains yielded the largest (~1.9-2.0-fold) increase of H_2 (~28.3 µmol/g

173   DW), followed by a 1.6-fold increase for the *gap1^{OEx}ΔldhA* strain. The initial H_2 production in the

174   first 1-2 days shows a faster rate for *ΔldhA* than the *gap1^{OEx}ΔldhA* and WT strains, indicating the

175   latter strains have a longer lag period before H_2 production. Bidirectional NiFe-hydrogenase is a

176   reversible enzyme and can oxidize the evolved H_2 to regenerate NADH for use in cellular

177   metabolism. To overcome this limitation partially, the headspace volume was increased to 15 mL,

178   keeping constant the number of cells as the 5-ml experiment (5 x 10^8 cells). Figure 2b compares

179   the H_2 yields after 3 d of autofermentation. Large increases in H_2 are clearly observed upon

180   increasing the headspace from 5 ml to 15 ml for all strains, which is consistent with decreasing H_2

181   uptake by cells through mass action. Under the 15 ml headspace volume, all three mutant strains

182   yielded significantly more H_2 than WT (0.16 ± 0.03 mol H_2/ mol glucose eq (Table 3)),

183   corresponding to increases of 4.6-fold *(Δgap1ΔldhA)*, 4.8-fold (*ΔldhA*), and 2.3-fold

184   (*gap1^{OEx}ΔldhA)*. The corresponding H_2/glucose eq yield of these strains is 1.32 %, 6.16 %, 6.41

185   %, and 3.13 % respectively (Table 3). Yield was calculated based on the percent theoretical

186   maximum of 12 mol H_2/ mol of glucose. As expected, all strains produced more H_2 using the larger

187   headspace compared to the 5-ml condition, ranging from the largest gain of 5.4-fold

188   (*gap1^OEx^ΔldhA), followed by a 4.8-fold (WT), 4.1-fold (Δgap1ΔldhA)* and 3.2-fold (*ΔldhA)*. The

189   consistency across all four strains supports the interpretation of H_2 uptake by the reversible

190   hydrogenase for metabolic utilization during autofermentation.

191

192   **Glycogen catabolic flux.**

193   Prior studies have shown that the loss of biomass during cyanobacterial autofermentation is almost

194   entirely from glycogen catabolism [24]. Hence, the amount of glycogen consumed during the dark

195   anoxic period was measured for batch cultures without H_2 milking. The rate of catabolism of total

196   reducing carbohydrate (TRC) were obtained from the slopes over 3 d (Figure 3).

197   At the start of autofermentation, representing the late-exponential phase of photoautotrophic

198   growth (at 1.2 OD_{730}), the total photoautotrophically accumulated carbohydrate measured as total

199   reducing sugar was identical for both WT and Δ*gap1*Δ*ldhA* strains (163.2 and 164.4 mg/g Dry

200   Weight (DW), respectively), while being 12.6 % greater for *gap1^OEx^*Δ*ldhA* strain (183.7 mg/g DW)

201   and 28.6 % lower for Δ*ldhA* cells (116.4 mg/g DW) (Figure 3, 0-h time point) compared to the

202   WT. Higher glycogen content in the *gap1^OEx^*Δ*ldhA* strain is in accordance with the previous report

203   of high glycogen accumulation in the GAPDH-1 overexpression (*gap1^OEx^)* strain [23].

204   During autofermentation, there was no correlation between the catabolic rate and the initial

205   glycogen content for the four strains. WT (90 μmol TRC/gDW/day) and *gap1^OEx^*Δ*ldhA* (94 μmol

206   TRC/gDW/day) cells have the fastest catabolic rate (indistinguishable) compared to the slower

207   rates for Δ*ldhA* (39 μmol TRC/gDW/day) and Δ*gap1*Δ*ldhA (*46 μmol TRC/gDW/day). The

208   autofermentative catabolic rate of glycogen is substantially lowered by the *ldhA* mutation (Figure

209   3). Furthermore, the catabolic rate was restored to the WT level by the overexpression of GAPDH-

210   1 in *gap1^OEx^*Δ*ldhA* (Figure 3). In conjunction with the total glycogen accumulated during the

211   photosynthetic phase, these results show that overexpression of GAPDH-1 allows for both faster

212   and greater gluconeogenesis in light (photoautotrophic growth) and faster and greater glycolytic

213   flux in dark anoxia (autofermentation).

214

215   **Pyridine nucleotide accumulation.**

216   Dark fermentative hydrogen production in cyanobacteria depends on the reductant produced

217   during catabolism. Therefore, the levels of pyridine nucleotides, adenylates and the catabolic

218   carbon metabolites were quantified using previously established protocols of LC-QQQ-MS[23].

219   After three days of autofermentation in 15 ml headspace experiment, all three mutant strains had

220   significantly smaller pool sizes of all the pyridine nucleotides compared to WT. The sum total pool

221   size of these pyridine nucleotides (NAD^+ + $NADP^+$ + NADPH + NADH) for $\Delta gap1\Delta ldhA$, $\Delta ldhA$,

222    $gap1^{OEx}\Delta ldhA$ and WT strains were 0.01, 0.03, 0.06, 0.1 mM/10^{17} cells, respectively. As expected

223   under autofermentative conditions, the NADH pool size was the largest fraction across all strains.

224   Compared to WT, the NADH levels decreased by 12.0 ($\pm$ 0.52), 4.0 ($\pm$ 0.25) and 2.2 ($\pm$ 0.17)-fold,

225   respectively (Figure 4a), and the NADPH levels decreased by 6.5 ($\pm$ 0.56), 5.9 ($\pm$ 1.6), and 3.4 ($\pm$

226   0.54)-fold for $\Delta gap1\Delta ldhA$, $\Delta ldhA$ and $gap1^{OEx}\Delta ldhA$, respectively (Figure 4a).

227   Though the levels of all pyridine nucleotides were lower in the mutants compared to WT,

228   the redox-poise ratios, NAD(P)H / NAD(P), were 4.1 ($\pm$ 0.44), 5.4 ($\pm$ 0.76), 13.5 ($\pm$ 1.2), and 4.5

229   ($\pm$ 0.24), (Figure 4b) for $\Delta gap1\Delta ldhA$, $\Delta ldhA$, $gap1^{OEx}\Delta ldhA$ and WT respectively. These results

230   indicate that all strains remain highly reduced with $gap1^{OEx}\Delta ldhA$ having significantly higher

231   NADH content than any of the other mutants (Fig 4b) and maintaining a 3-fold higher total redox

232   charge than the remaining strains. This outcome is consistent with larger glycogen pool size and

233   greater catabolic flux in this mutant. In addition, $\Delta gap1\Delta ldhA$ showed higher NADPH/NADP ratio

234   (Fig 4b inset) and the lowest NADH/ NAD ratio as compared to the remaining tested strains.

235

236   **Cellular energy content.**

237   Like the total pyridine nucleotide pool size, all three mutant strains had significantly smaller total

238   adenylate pool sizes (ATP + ADP + AMP) after 3 d of dark fermentative conditions (Figure 5).

239   The total pool size ranks in increasing order $\Delta gap1\Delta ldhA$ < $gap1^{OEx}\Delta ldhA$ < $\Delta ldhA$ << WT (0.02,

240   0.03, 0.05 and 0.4 mM/10^{17} cells, respectively). As expected, the dominant influence was observed

241   after deletion of $ldhA$. As lactate dehydrogenase uses pyruvate, the product of both the glycolytic

242   and OPP pathways, its absence is expected to dominate over that of upstream changes at GAPDH.

243   Although, all three mutant strains had smaller adenylate pools, they had significant but much

244   smaller differences in their cellular energy charge of 0.2, 0.2 and 0.3 respectively, compared to 0.1

245   for WT. Cellular energy charge, CEC, calculated as CEC = (ATP + (0.5 ADP))/(ATP + ADP +

246   AMP) is a measure of the metabolically available energy that is transiently stored in the adenylate

247   system[33].

248

249   **Carbon metabolite levels.**

250   To understand the consequences of the genetic modifications introduced in the glycolytic pathway,

251   the pools of glycolytic metabolites were measured in the WT and mutant strains after 72 h of

252   autofermentation using LC-QQQ-MS (Figure 6). While compared to WT, the *ldhA* mutant strain

253   exhibits a lower glycolytic rate, it has significantly higher accumulation of all the upper-glycolysis

254   intermediates immediately prior to GAPDH-1(from glyceraldehyde 3 phosphate (GAP) and

255   above), and significantly reduced levels of lower-glycolysis intermediates, except 3PG (1.4-fold

256   higher). This outcome is expected as the accumulation of excess NAD(P)H, expected from the

257   deletion of *ldhA*, slows the glycolytic flux through the $NAD(P)^+$-dependent bottleneck step,

258   GAP→1,3-bisphosphoglycerate, which is catalyzed by GAPDH-1 [34], [23].

259

260   Modifying glycolysis by deletion of the *gap1* gene is expected to reroute carbohydrate catabolism

261   through the OPP pathway, while *gap1* overexpression is expected to increase the flux through

262   glycolysis, assuming downstream steps are not limiting. Removing GAPDH-I from the Δ*ldhA*

263   background in the double knockout strain, Δ*gap1*Δ*ldhA*, gives a similar overall profile with slightly

264   reduced upper-glycolysis intermediates, except for GAP accumulation compared to Δ*ldhA* (Figure

265   6). Adding overexpression of the *gap1* gene to this background, the *gap1*^{OEx}Δ*ldhA* strain shows a

266   profile like Δ*gap1*Δ*ldhA*, but with significantly decreased GAP level, yet still higher than WT. The

267   former outcome is consistent with the expected opening of the metabolic bottleneck at GAPDH-

268   1, while the later outcome shows the influence of the loss of the lactate sink.

269

270   **Irreversible H_2 production under continuous milking.**

271   As diluting the H_2 concentration in the headspace by increasing headspace volume led to a

272   significant increase in the total H_2 production (Figure 2b), we conclude that hydrogenase is poised

273   to perform the H^+ reduction reaction rather than H_2 oxidation. To test this hypothesis and boost H_2

274   production further, we applied electrochemical milking to consume dissolved H_2 from the culture

275   medium using a tiny volume of cells to shift the equilibrium further and maximize H_2 production

276   (Figure 7a). H_2 is oxidized electrochemically, and thus the real-time rates of H_2 production are

277   directly proportional to the measured current. Integration gives the H_2 yield in the closed cell. H_2

278   was measured using a home-built rate electrode comprised of a 4 mm diameter Pt-Ir electrode

279   covered by a ultrathin membrane (0.3 to 1 micron thick) upon which is layered a small culture

280   volume (8 µl) and sealed by glass cover and Teflon ring[24]. In the same cell, we simultaneously

281   measured continuously the concentration of NAD(P)H by its inherent fluorescence (Figure 7b).

282   The total hydrogen yield was calculated as described in the Experimental section. Glycogen

283   consumed before and after 20 h of fermentation was also measured from the experimental sample.

284   Similar to vial experiments, glycogen consumption was highest in WT and *gap1^{OEx}ΔldhA,* 108.9

285   µmol TRC /g DW and 104.7 µmol TRC /g DW followed by Δ*gap1*Δ*ldhA* (88.8 µmol TRC /g

286   DW) and Δ*ldhA* (65.2 µmol TRC /g DW).

287   The H$_2$ rate and NAD(P)H concentration data reveal a reciprocal relationship in each strain

288   (Figure 7a and b). WT has the lowest H$_2$ production rate, and as fermentation develops, it retains

289   the highest NAD(P)H concentration. The double knockout strain starts slowly but develops the

290   highest H$_2$ production rate, while the NAD(P)H level starts higher and depletes to very low level

291   in synchrony with the H$_2$ evolution rate. A consistent picture emerges across all four strains

292   demonstrating that elimination of equilibrium conditions by continuous removal of H$_2$ lowers the

293   intracellular level of NAD(P)H proportionately.

294   The rate of H$_2$ production averaged over the initial 20 h of autofermentation is summarized

295   in Figure 7c for all four strains. To normalize to per day basis, the average rate of H$_2$ produced per

296   hour was multiplied by 24. The resulting daily average H$_2$ production rates decrease in order (µmol

297   H$_2$/g DW/day): Δ*gap1*Δ*ldhA* (680) > *gap1^{OEx}*Δ*ldhA (*333) > Δ*ldhA* (265) > WT (94). Relative to

298   the WT strain, the mutants exhibit greater H$_2$ production rates by 7.2-, 3.5- and 2.8-fold under

299   milking conditions. The yield of hydrogen under milking conditions is reported in Table 3, which

300   was derived by normalizing to the glycogen consumed during electrochemical milking of H$_2$. The

301   yield from milking conditions is compared to the non-milking conditions in Table 3. The yields

302   under milking conditions are 53.3 % for Δ*gap1*Δ*ldhA*, 28.3% for Δ*ldhA* 22.2% for *gap1^{OEx}*Δ*ldhA*

303   and 6.1 % for WT. The fact that the yield of Δ*gap1*Δ*ldhA* is significantly higher than the 33% yield

304   of the Thauer limit indicates that there is a very substantial contribution from the OPP or alternate

305   pathways towards reductant generation in this strain. Thus, it is possible to cross the Thauer limit

306   *in vivo* by rewiring two key pyridine nucleotide-dependent steps of central carbon metabolism with

307   concomitant elimination of hydrogen uptake.

308

309   **Discussion**

310   Photosynthetically accumulated glycogen is the storage product of atmospheric carbon

311   dioxide and hydrogen derived from photosynthetic water oxidation carried by NADPH. It can be

312   catabolized to extract carbon intermediates, redox energy and ATP either via glycolysis (Embden-

313   Meyerhof-Parnas) or the OPP pathway, forming different products and yields (Figure 1a).

314   Glycolysis is overwhelmingly favored over OPP during dark anaerobiosis as it is the only source

315   of ATP when respiration is prevented. In such cases, hydrogenase functions as terminal oxidase to

316   regenerate NAD(P)$^+$ by consuming *excess* NAD(P)H (venting H$_2$ gas) that is not used to produce

317   metabolites. Accordingly, it is a redox safety valve of variable yield but is not an obligatory product

318   of glycogen catabolism. Hence, the challenge for maximizing glycogen-derived fermentative H$_2$

319   production is stripping hydrogen from carbon intermediates (maximizing CO$_2$ release), while still

320   creating sufficient cellular energy as ATP.

321   *Synechococcus* 7002 is an oxygenic photoautotrophic cyanobacterium with the ability to

322   produce molecular hydrogen anaerobically via autofermentation using an O$_2$-sensitive NiFe-

323   hydrogenase and hydrogen derived from NAD(P)H [16]. In addition to producing H$_2$, *Synechococcus*

324   7002 also excretes lactate, acetate, alanine and carbon dioxide under autofermentative conditions

325   (Figure 1a). Among these, lactate is the predominant fermentative end product in this

326   cyanobacterium; its synthesis mainly recycles NAD$^+$ needed to sustain glycolysis which generates

327   ATP[16]. Because lactate is the major carbon and reductant sink under fermentative conditions, LDH

328   is the major competitor for electrons with hydrogenase[16]. Previously, it was demonstrated that

329   knocking out GAPDH-1 in *Synechococcus* 7002 resulted in an increased NAD(P)H level and faster

330   rate of H$_2$ evolution under autofermentation[23]. This was shown to be due to rerouting of glycogen

331   catabolism via the OPP pathway. Curiously, overexpression of the same gene also produced more

332   autofermentative H$_2$ than WT, which was shown to be due to the combined effects of opening the

333   rate-limiting bottleneck in glycolysis at GAPDH-1, in combination with the accumulation of

334   significantly more glycogen (NAD(P)H precursor) during the prior photoautotrophic growth stage.

335   Both mutations also produced similar or higher levels of lactate compared to WT[23]. Therefore,

336   with an aim to boost H$_2$ production even further, herein we engineered two double-mutant cell

337   lines containing both *ldhA* knock-out and either knock-out or overexpression of *gap1*. Our

338   rationale was to: a) eliminate the competition for reductant (*ldhA* deletion), b) enhance NAD(P)H

339   production (*gap* mutants), and c) eliminate H$_2$ uptake by NiFe-hydrogenase using electrochemical

340   milking. By quantitatively measuring the reductant sources continuously (H$_2$ and NAD(P)H) and

341   the concentrations of intermediates of central carbon metabolism during autofermentation, we

342   could delineate the metabolic pathways affected in these mutants and follow the fluxes in realtime.

343   Under a fixed headspace volume, both mutant strains $\Delta ldhA$ and $\Delta gap1\Delta ldhA$ had

344   significantly lower glycogen catabolic rates compared to WT. LDH, the main redox-balancing

345   enzyme during fermentation in *Synechococcus* 7002 [16], not only recycles NAD^+, but also converts

346   pyruvate produced by glycolysis into the terminal carbon sink, lactate, which is excreted.

347   Monitoring of both processes shows that these processes are restricted in the *ldhA* mutant strain,

348   which accounts for the lower rate of glycogen catabolism. The combined observations of the lower

349   rate of glycogen catabolism in $\Delta gap1\Delta ldhA$ and the higher $NADPH/NADP^+$ ratio, suggests that

350   although OPP is operating in the mutant, the flux is inefficient under the experimental conditions

351   of accumulating headspace H_2. A potential cause might be the higher $NADPH/NADP^+$ ratio in this

352   mutant (Figure 4b) which can allosterically down-regulate the G6PDH, enzyme involved in the

353   first step of the OPP pathway[35, 36]. However, by "milking" to remove H_2, this ratio is lowered, and

354   down-regulation is overcome thereby allowing greater carbon flux through OPP (Table 3, Figure

355   7).

356   In the case of $gap1^{OEx}\Delta ldhA$, a strain engineered for increased gluconeogenesis and

357   glycolysis rates, enhanced glycogen production (11-17% more glycogen) was observed during

358   photoautotrophic growth, but this strain showed no significant difference in glycogen catabolism

359   rate compared to WT. However, gluconeogenesis was significantly faster than the *ldhA* deletion

360   mutant which accumulated 38% less glycogen during photosynthesis. The metabolite data (Figure

361   6) suggests the unchanged catabolic rate in $gap1^{OEx}\Delta ldhA$ could be a result of the higher

362    $NADH/NAD^+$ ratio and a lower total NAD(H) availability. We know that removing LDH-

363   dependent reoxidation of NADH results in a higher redox charge and expect this may lead to

364   substrate-level inhibition of GAPDH-1 (Figure 4), with a concomitant net slowing of the overall

365   glycolysis rate. A similar mechanism of NADH-dependent inhibition of GAPDH has been

366   postulated previously in *Lactococcus lactis*[34].

367   Owing to the bidirectional nature of hydrogenase and the unfavorable electrochemical

368   potential difference of 100 mV between the H_2/H^+ couple and the NADH/NAD couple[37], NiFe-

369   hydrogenase alone is insufficient to reoxidize the accumulated NAD(P)H to $NAD(P)^+$ under a

370   fixed headspace volume (Figure 4b). With a 5-mL headspace volume, both $gap1^{OEx}\Delta ldhA$ and

371    $\Delta gap1\Delta ldhA$ showed no increase in their H_2 production compared to *ldhA* mutant strain (Figure

372 2b), and was much lower compared to the cumulative yields of the individual *gap1* mutant(s)[16, 23].

373 Upon combining these mutations, the unchanged levels of H_2 in addition to the higher redox poise

374 indicate the inability of such strains to utilize the available reductant owing to a kinetic barrier.

375 Presumably, intracellular H_2 oxidation reaches equilibrium and prevents further increases in H_2

376 concentration. This prediction was verified by increasing the headspace volume to 15 mL, resulting

377 in substantial (> 3-fold) increase of H_2 for all strains. The three mutant strains showed substantially

378 decreased amounts of lower-glycolysis intermediates and increased accumulation of upper-

379 glycolysis intermediates above the GAPDH-1 bottleneck (Figure 6). This phenotype is expected

380 for the double knockout mutant Δ*gap1*Δ*ldhA*, as it was engineered to utilize the OPP pathway

381 rather than glycolysis. As expected, an analogous phenotype was observed for the (single) *gap1*

382 knockout mutant in our earlier study[23]. Observation of the analogous phenotype in the single

383 mutant Δ*ldhA* may be similarly explained, because the significantly elevated NADH/NAD ratio

384 (~6) will inhibit net glycolytic flux through GAPDH-1.

385 The electrochemical milking strategy was used to overcome these limitations so that the

386 increased NAD(P)H levels could be channeled into H_2 production and reveal the inherent capacity

387 of the given genetic modifications to affect H_2 production (Figure 7). The WT strain can produce

388 the largest NAD(P)H increase in concentration but cannot convert the increased reductant charge

389 into higher yields of H_2. Among the four strains, the Δ*gap1*Δ*ldhA* strain exhibits the largest

390 NAD(P)H/NAD(P) ratio (1.5 fold more than WT) after anaerobiosis is quickly attained, and it

391 maintains a constant, high level for 5 h during H_2 milking in contrast to the other strains (Figure

392 7b). This feature is evidence that this mutant uses additional pathways for its glycogen catabolism

393 other than those available for the Δ*ldhA* and *gap1*^{OEx}Δ*ldhA* strains. Following this 5-h period

394 during which the glycolytic enzymes are expressed/activated, the H_2 production rate in the

395 Δ*gap1*Δ*ldhA* strain increased continuously, while concomitant oxidation of the NAD(P)H

396 decreases its intracellular concentration. After reaching its maximum H_2 production rate at 16 h

397 and decreasing thereafter, the strain had reached a minimum in the NAD(P)H concentration. As

398 the latter concentration is the result of its net production and consumption rates, the combined data

399 indicate that the rate of hydrogenase-dependent production of intracellular H_2 accelerates over the

400 initial 16-h period. Hydrogen production in this strain occurred at an average rate of 680 μmol

401 H_2/g DW/day, compared to the nearly 3-fold lower rates for the *gap1*^{OEx}Δ*ldhA* and Δ*ldhA* strains.

402 This corresponds to a stoichiometry of 6.4 mol H_2/mol glucose and an integrated yield of 53.3%

403 over the period of 20 h of the milking experiment (Figure 7c; Table 3).

404 The Thauer limit for maximum H_2 yield via glycolysis is 4 H_2 per glucose. Thus, a yield

405 of 6.4 H_2 per glucose indicates the ability of the $\Delta gap1\Delta ldhA$ strain to use the OPP pathway or

406 other additional NAD(P)H generating pathways which can produce more than 4 moles of

407 NAD(P)H/mol of glucose. The higher yield in $\Delta gap1\Delta ldhA$ under milking conditions probably

408 occurs by overcoming the NADPH-dependent inhibition of G6PDH with a continuous oxidation

409 of NADPH by NiFe-hydrogenase. To our knowledge, this is the highest yield of H_2 reported for

410 any phototrophic or heterotrophic bacterium reported so far [23, 31].

411 Under continuous H_2 milking conditions, the WT strain accumulated high levels of

412 NAD(P)H but produced the least amount of H_2 compared to the engineered mutant strains. WT

413 could not utilize the available NAD(P)H for H_2 production. The simplest explanation is that WT

414 cells have a functional LDH enzyme, which converts pyruvate to lactate using NADH at a

415 significantly more positive redox potential than required for hydrogenase to convert H^+ to H_2[16].

416 Hence, by normally having both LDH and GAPDH-1, the WT strain can prevent the loss of

417 valuable intracellular reducing power over a much wider range of NAD(P)H/NADP$^+$ ratios, even

418 under continuous H_2 removal conditions in natural environments.

419

420 **Conclusion**

421 In conclusion, these results demonstrate the plasticity of central carbon metabolism in

422 cyanobacteria to accommodate large changes in carbon and hydrogen fluxes in engineered strains.

423 The major impact of product removal on *in vivo* autofermentation rate is quantitatively

424 demonstrated. The future focus should be on both process engineering as well as converting or

425 replacing the bidirectional NiFe-hydrogenase with an unidirectional enzyme that acts

426 preferentially to reduce protons. Additionally, the *in vivo* approach for H_2 generation allows for

427 exploiting the viability of cells by cell recycling post production, thus lowering the time and cost

428 of production.

429

430 **Conflicts of interest**

431 There are no conflicts to declare.

432

1

References:

1.   SMRCPL, *Hydrogen Generation - Global Market Outlook (2017-2026)*, 2018.
2.   G. F. Naterer, Jaber, O., Dincer, I., Essen, 2010.
3.   EIA, *Journal*, 2018.
4.   P. C. Hallenbeck and J. R. Benemann, *International Journal of Hydrogen Energy*, 2002, **27**, 9.
5.   C. Ding, K. L. Yang and J. He, in *Handbook of Biofuels Production (Second Edition)*, eds. R. Luque, C. S. K. Lin, K. Wilson and J. Clark, Woodhead Publishing, 2016, DOI: https://doi.org/10.1016/B978-0-08-100455-5.00011-4, pp. 303-333.
6.   M. L. Ghirardi, M. C. Posewitz, P. C. Maness, A. Dubini, J. Yu and M. Seibert, *Annu Rev Plant Biol*, 2007, **58**, 71-91.
7.   E. Aubert-Jousset, M. Cano, G. Guedeney, P. Richaud and L. Cournac, *FEBS J*, 2011, **278**, 4035-4043.
8.   L. Cournac, G. Guedeney, G. Peltier and P. M. Vignais, *Journal of Bacteriology*, 2004, **186**, 1737-1746.
9.   D. Carrieri, K. Wawrousek, C. Eckert, J. Yu and P. C. Maness, *Bioresour Technol*, 2011, **102**, 8368-8377.
10.   K. Gutekunst, X. Chen, K. Schreiber, U. Kaspar, S. Makam and J. Appel, *J Biol Chem*, 2014, **289**, 1930-1937.
11.   A. Krishnan, X. Qian, G. Ananyev, D. S. Lun and G. C. Dismukes, in *Synthetic Biology of Cyanobacteria*, eds. W. Zhang and X. Song, Springer Singapore, Singapore, 2018, DOI: 10.1007/978-981-13-0854-3_8, pp. 171-213.
12.   S. Kim, E. Seol, Y.-K. Oh, G. Y. Wang and S. Park, *International Journal of Hydrogen Energy*, 2009, **34**, 7417-7427.
13.   J. Woodward, M. Orr, K. Cordray and E. Greenbaum, *Nature*, 2000, **405**, 1014-1015.
14.   R. K. Thauer, K. Jungermann and K. Decker, *Bacteriological Reviews*, 1977, **41**, 100-180.
15.   L. J. Stal and R. Moezelaar, *Fems Microbiology Reviews*, 1997, **21**, 179-211.
16.   K. McNeely, Y. Xu, N. Bennette, D. A. Bryant and G. C. Dismukes, *Appl Environ Microbiol*, 2010, **76**, 5032-5038.
17.   P. C. Hallenbeck, M. Abo-Hashesh and D. Ghosh, *Bioresource technology*, 2012, **110**, 1-9.
18.   P. C. Hallenbeck and D. Ghosh, *J Environ Manage*, 2012, **95**, S360-S364.
19.   W. Khetkorn, N. Khanna, A. Incharoensakdi and P. lindblad, *Biofuels*, 2013, **4**, 535-561.
20.   W. Baebprasert, S. Jantaro, W. Khetkorn, P. Lindblad and A. Incharoensakdi, *Metab Eng*, 2011, **13**, 610-616.
21.   X. Qian, G. K. Kumaraswamy, S. Zhang, C. Gates, G. M. Ananyev, D. A. Bryant and G. C. Dismukes, *Biotechnol Bioeng*, 2016, **113**, 979-988.
22.   A. A. Shestov, X. Liu, Z. Ser, A. A. Cluntun, Y. P. Hung, L. Huang, D. Kim, A. Le, G. Yellen, J. G. Albeck and J. W. Locasale, *Elife*, 2014, **3**.
23.   G. K. Kumaraswamy, T. Guerra, X. Qian, S. Zhang, D. A. Bryant and G. C. Dismukes, *Energy and Environmental Science*, 2013, **6**, 3722-3731.
24.   G. M. Ananyev, N. J. Skizim and G. C. Dismukes, *J Biotechnol*, 2012, **162**, 97-104.
25.   N. J. Skizim, G. M. Ananyev, A. Krishnan and G. C. Dismukes, *J Biol Chem*, 2012, **287**, 2777-2786.

26.   M. H. Zwietering, I. Jongenburger, F. M. Rombouts and K. van 't Riet, *Appl Environ Microbiol*, 1990, **56**, 1875-1881.
27.   Y. Xu, R. M. Alvey, P. O. Byrne, J. E. Graham, G. Shen and D. A. Bryant, *Methods Mol Biol*, 2011, **684**, 273-293.
28.   A. Krishnan, S. Zhang, Y. Liu, K. A. Tadmori, D. A. Bryant and C. G. Dismukes, *Biotechnol Bioeng*, 2016, **113**, 1448-1459.
29.   W. E. Trevelyan and J. S. Harrison, *The Biochemical journal*, 1952, **50**, 298-303.
30.   N. B. Bennette, J. F. Eng and G. C. Dismukes, *Analytical chemistry*, 2011, **83**, 3808-3816.
31.   G. Ananyev, D. Carrieri and G. C. Dismukes, *Appl Environ Microbiol*, 2008, **74**, 6102-6113.
32.   G. Korotcenkov, S. D. Han and J. R. Stetter, *Chem Rev*, 2009, **109**, 1402-1433.
33.   A. G. Chapman, L. Fall and D. E. Atkinson, *J Bacteriol*, 1971, **108**, 1072-1086.
34.   C. Garrigues, M. Mercade, M. Cocaign-Bousquet, N. D. Lindley and P. Loubiere, *Biotechnol Bioeng*, 2001, **74**, 108-115.
35.   F. Schaeffer and R. Y. Stanier, *Archives of microbiology*, 1978, **116**, 9-19.
36.   R. A. Pelroy, M. R. Kirk and J. A. Bassham, *Journal of bacteriology*, 1976, **128**, 623-632.
37.   P. Tamagnini, E. Leitao, P. Oliveira, D. Ferreira, F. Pinto, D. J. Harris, T. Heidorn and P. Lindblad, *FEMS Microbiol Rev*, 2007, **31**, 692-720.
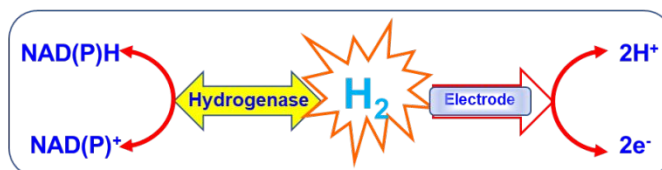
Fig. 1a)
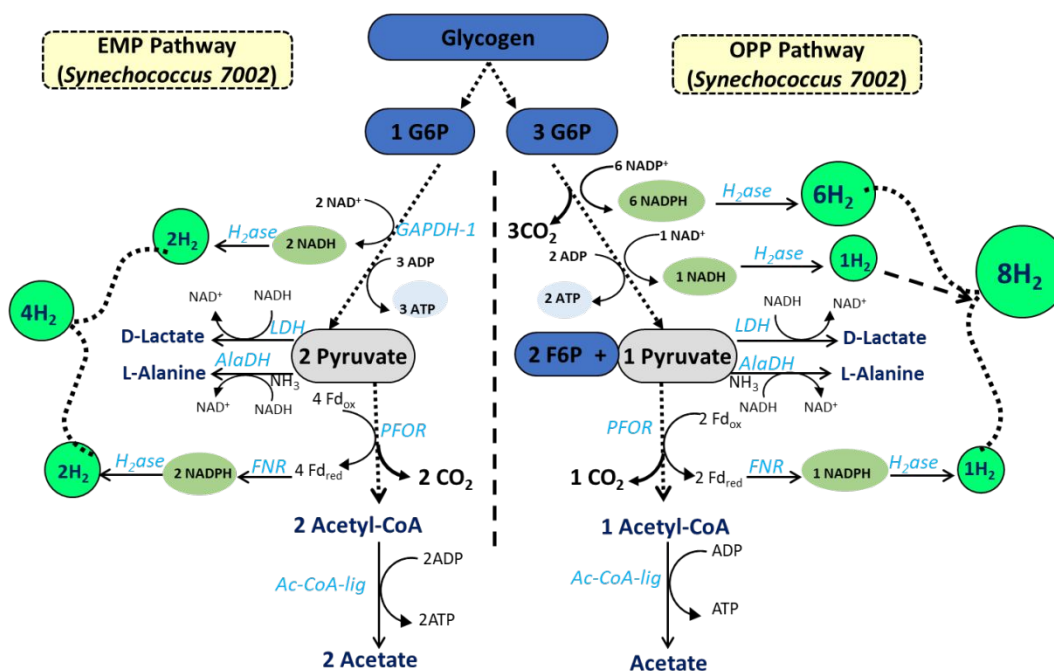
Figure 1a: Metabolic pathways leading to H_2 in cyanobacterium *Synechococcus 7002*. Oxidative pentose phosphate pathway (OPP) + lower glycolysis, Emden-Meyerhoff-Parnas pathway (EMP) + lower glycolysis, Glucose 6-phosphate (G6P), Fructose 6-phosphate (F6P), glyceraldehyde 3-phosphate dehydrogenase (GAPDH-1), hydrogenase (H_2ase), lactate dehydrogenase (LDH), alanine dehydrogenase (AlaDH), pyruvate ferrodoxin oxidoreductase (PFOR), Acetyl-CoA ligase (Ac-CoA-lig), ferredoxin-NADP oxidoreductase (FNR) **b)** Electrochemical "H_2 milking" by conversion of bidirectional NiFe-hydrogenase to unidirectional NiFe-hydrogenase, using membrane-covered biased electrode (poised at +220 mV 169 vs. Ag/AgCl in 100 mM KCl) to oxidize H_2.

2
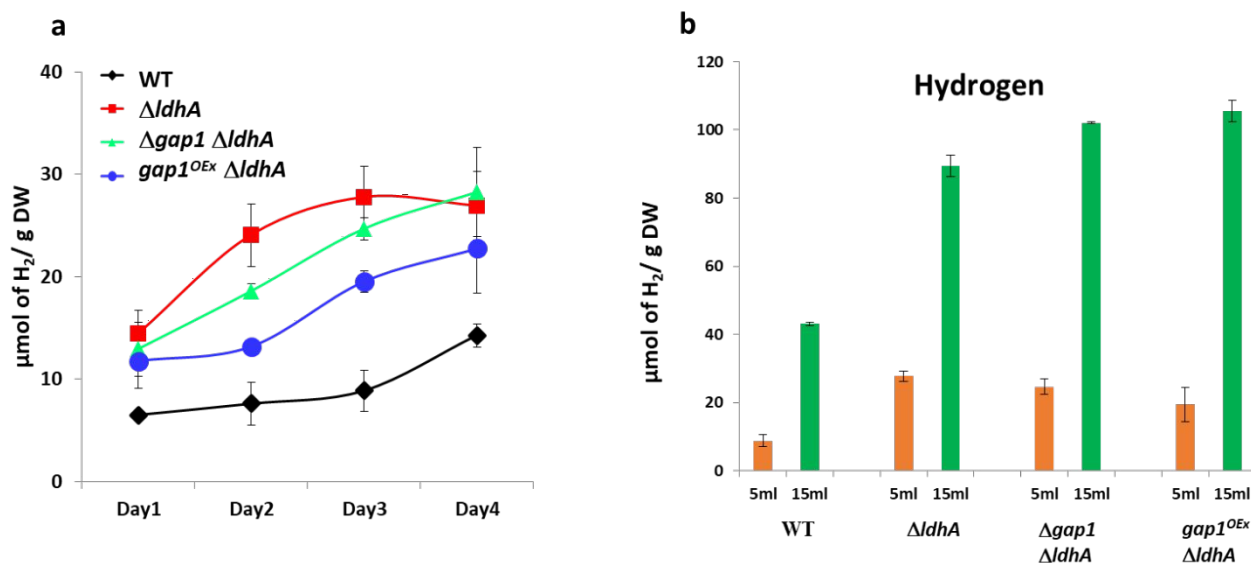
Figure 2: a) H_2 yields per dry weight of cells for WT, $\Delta ldhA$, $\Delta gap1\Delta ldhA$, and $gap1^{OEx}\Delta ldhA$ strains of *Synechococcus* 7002 over four days of dark anaerobic conditions under 5 mL of fixed headspace volume and no H_2 milking. Data based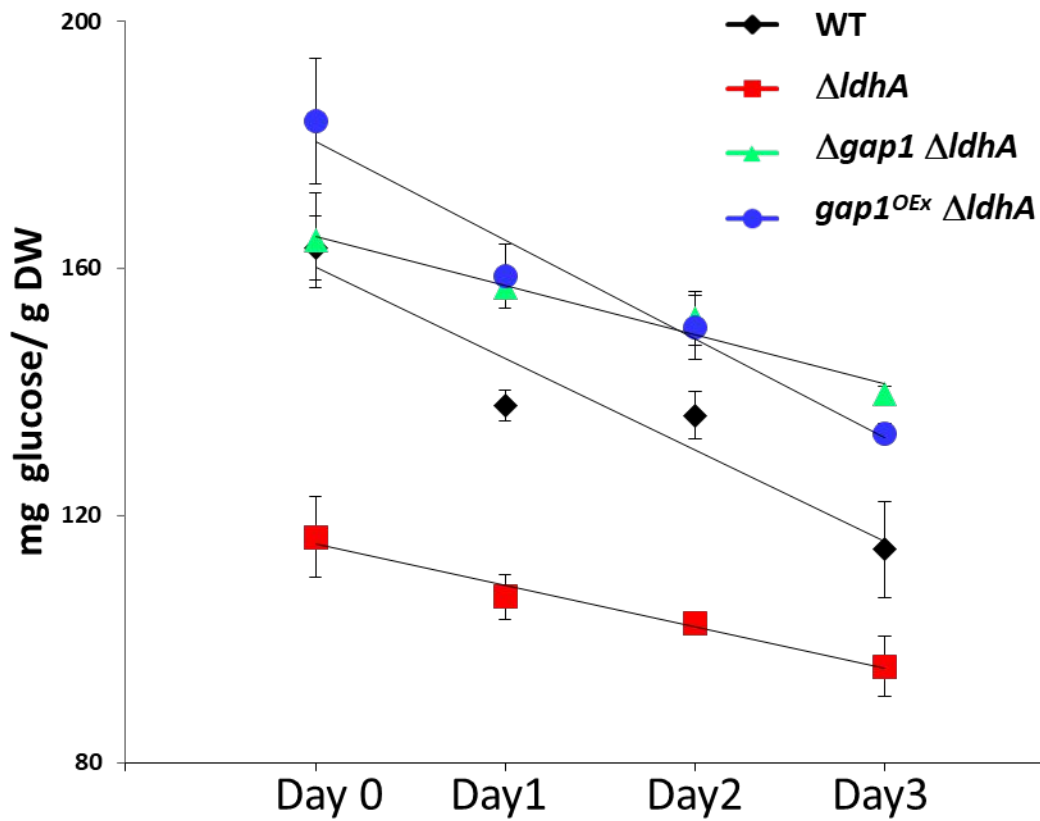 on 3 biological replicates with standard error. **b)** Headspace H_2 yields of WT, $\Delta ldhA$, $\Delta gap1\Delta ldhA$, and $gap1^{OEx}\Delta ldhA$ strains of *Synechococcus* 7002 after 3 days of dark anaerobic conditions under 5 mL and 15 mL of fixed headspace volume. Data based on 4 biological replicates with standard error.

2

Figure 3: Carbohydrate content of cells following initiation of dark anaerobiosis over 3 days from WT, $\Delta ldhA$, $\Delta gap1\Delta ldhA$, and $gap1^{OEx}\Delta ldhA$ strains of *Synechococcus* 7002 under 15 mL fixed headspace volume and no H_2 milking. The intracellular glycogen content was measured as the total reducing carbohydrate by anthrone assay using four biological replicates.
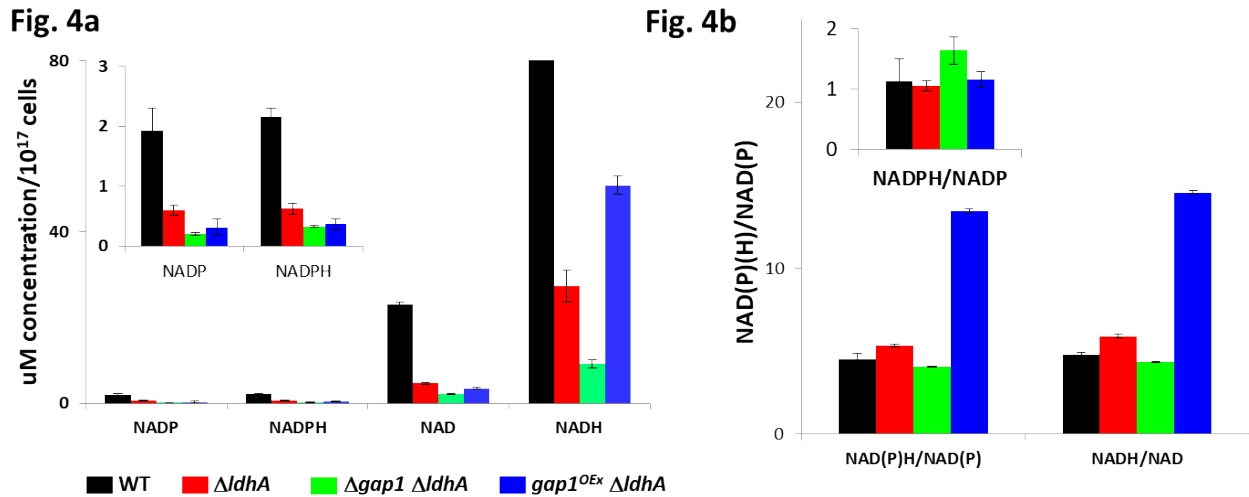
Figure 4 (a): Intracellular pyridine nucleotide concentrations of WT, Δ*ldhA,* Δ*gap1*Δ*ldhA*, and *gap1*^{OEx}Δ*ldhA* strains of *Synechococcus* 7002 after 3 days of dark fermentative conditions same as in Figure 3. Inset shows a magnified view of NADP$^+$ and NADPH **(b):** Reduced/oxidized ratio of pyridine nucleotide pairs. NAD(P)H/NAD(P) is the ratio of the sum of both pairs. Intracellular metabolite pools were determined using LC-QQQ-MS.
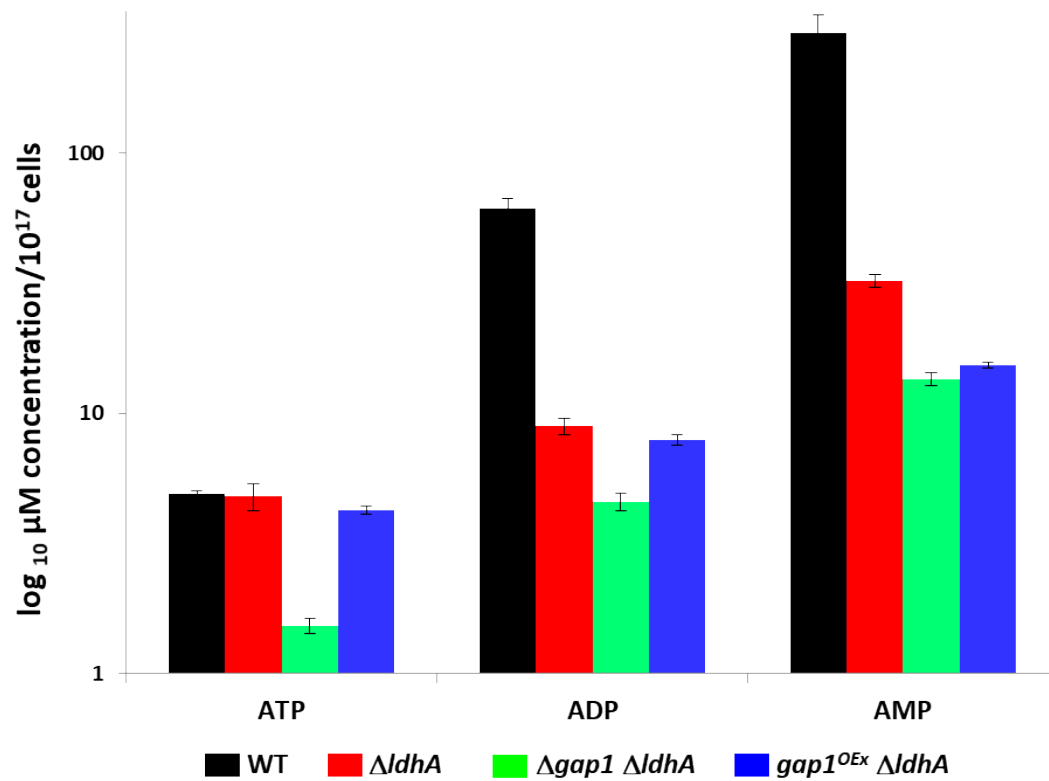
Fig. 5

Figure 5: Intracellular adenosine phosphate concentrations of WT, Δ*ldhA,* Δ*gap1*Δ*ldhA* and *gap1^{OEx}*Δ*ldhA* strains of *Synechococcus* 7002 after 3 days of dark fermentative conditions. Conditions as in Figure 3.

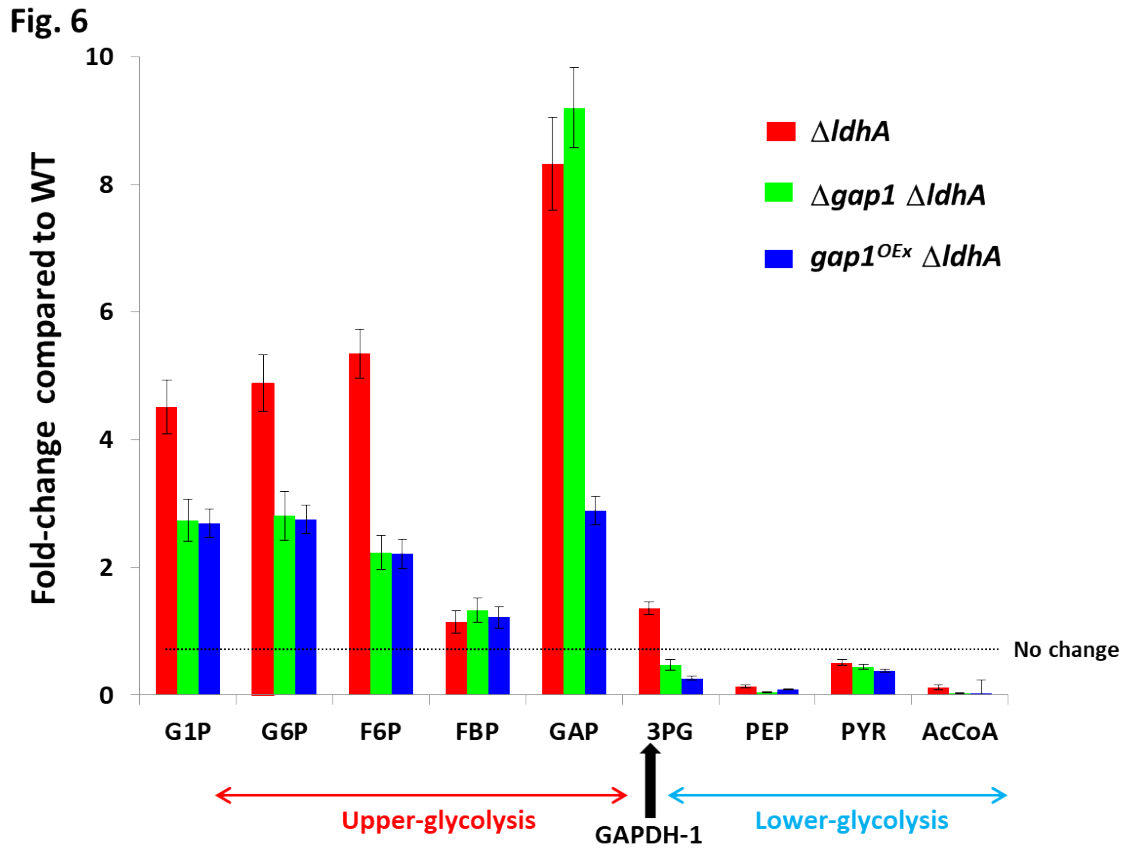**Figure 6:** Change in concentration of intracellular glycolytic metabolites (fold-change) of Δ*ldhA*, Δ*gap1*Δ*ldhA* and *gap1*^*OEx*Δ*ldhA* strains of *Synechococcus* 7002 compared to WT strain after 3 days of dark autofermentation. Conditions as in Figure 3. Metabolites were determined using LC-QQQ-MS. G1P= glucose-1-phosphate; G6P= glucose-6-phosphate; F6P= fructose-6-phosphate; FBP= fructose-1,6-bis phosphate; GAP= glyceraldehyde-3-phosphate; 3PG= 3-phosphoglycerate; PEP = phosphoenolpyruvate; Pyr = pyruvate; AcCoA = acetyl coenzyme A.
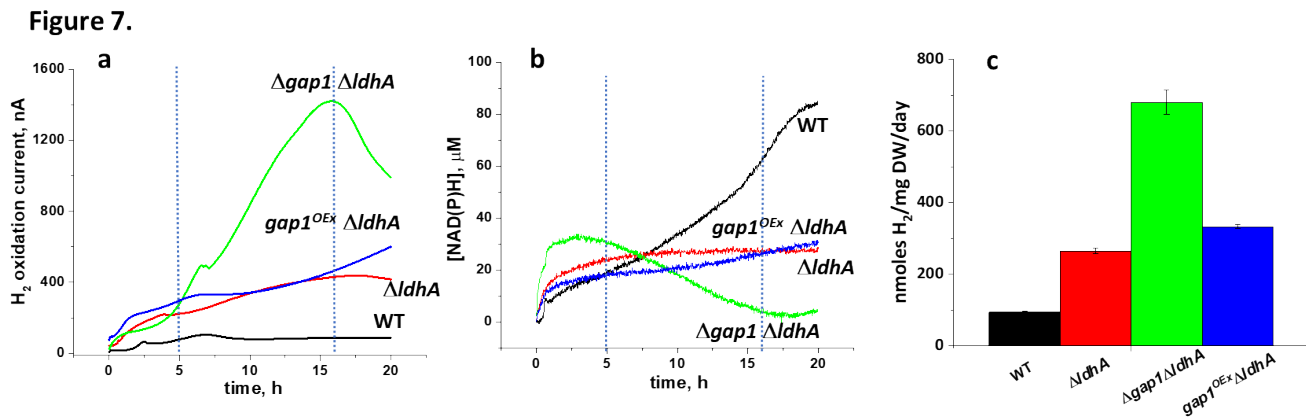
Figure 7.

Figure 7: Simultaneous realtime determination of the extracellular H_2 oxidation current density **(a)** and the intracellular NAD(P)H fluorescence intensity converted to concentration **(b)** of *Synechococcus* 7002 cells during autofermentation of internal glycogen stores over 20 hrs of continuous H_2 consumption by milking. Comparison of four strains: WT, *ΔldhA, Δgap1ΔldhA*, and *gap1^{OEx}ΔldhA*. **(c):** Average H_2 production rates from integrated current densities in (a). All H_2 is consumed electrochemically using a thin membrane-covered electrode, "H_2 milking conditions**".**
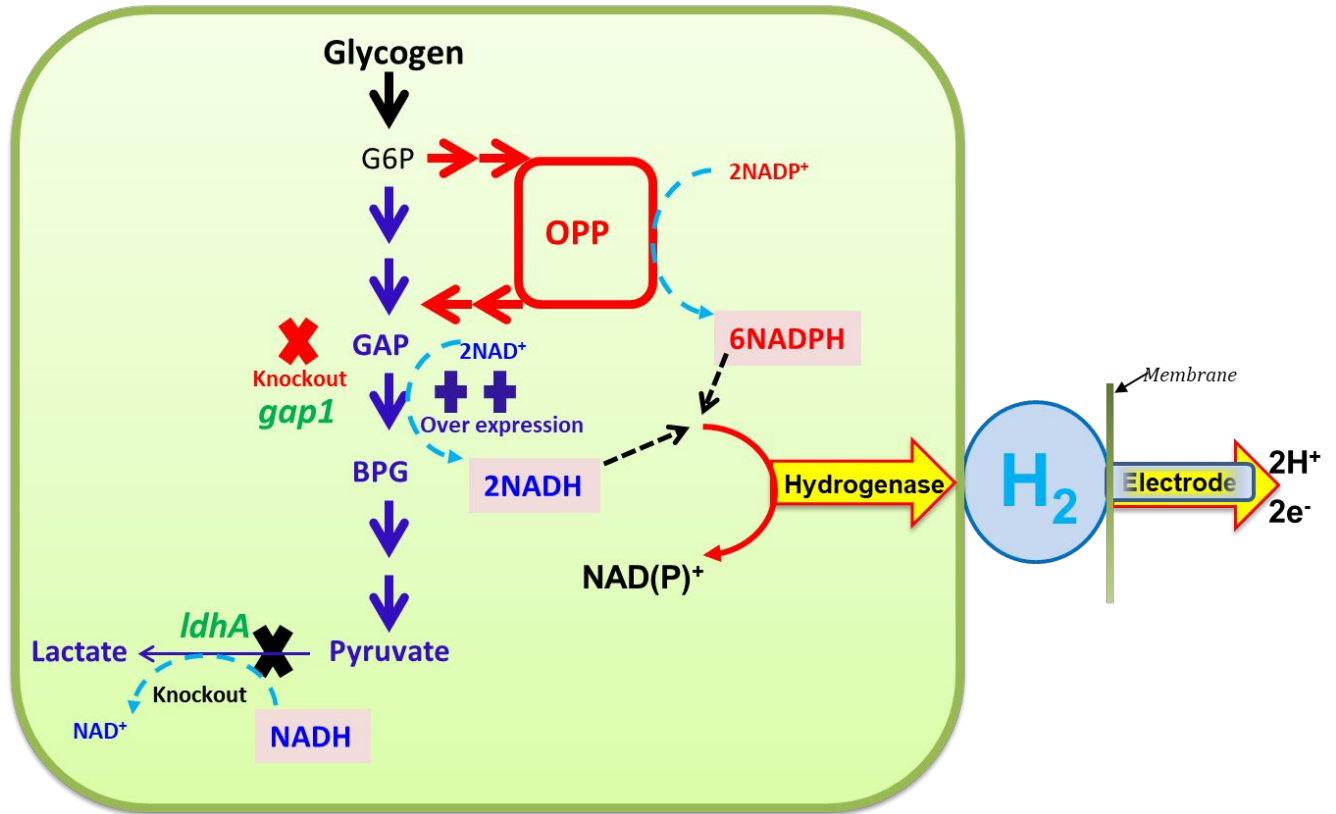
2

Figure 8: Metabolic engineering to enhance NAD(P)H production coupled with electrochemical milking for increased H_2 production rate and yield in *Synechococcus* 7002 WT and mutants. Gene knockout (X) and overexpression (++) targets and pyridine nucleotide stoichiometries are denoted.

Table 1. Strains and plasmids used in this study.

Strains/plasmid name	Genotype	Resistance marker[1]	Reference
Synechococcus 7002	Wild type cyanobacterium *Synechococcus* sp. PCC 7002		
Δ*ldhA*	*Synechococcus 7002, ldhA::aacC1*	Gm	[16]
Δ*gap1*	*Synechococcus 7002, Δgap1::aphII*	Km	[23]
gap1[OEx]	*Synechococcus 7002, Δgap1::aphII*, pAQ1-Ex*::gap1*	Km Sp	[23]
Δ*gap1* Δ*ldhA*	*Synechococcus 7002, ldhA::aacC1, Δgap1::aphII*	Gm Km	This study
gap1[OEx] Δ*ldhA*	*Synechococcus 7002, ldhA::aacC1, Δgap1::aphII,* pAQ1-Ex*::gap1*	Gm Km Sp	This study
pAQ1-Ex*::gap1*	Plasmid, pAQ1-Ex*::P$_{cpcBA}$::gap1*	Sp	[23]

[1]Gm, gentamicin; KmR, kanamycin; Sp, spectinomycin.

Table 2. Photoautotrophic growth rate of WT, $\Delta ldhA$, $\Delta gap1\Delta ldhA$, and $gap1^{OEx}\Delta ldhA$ strains of *Synechococcus* 7002, grown under 38 °C with a light intensity of 200 μmol photons $m^{-2} s^{-1}$ sparged with 2% (v/v) CO_2 in air. Growth rates were calculated by fitting the data to Gompertz function.

Strain	Growth Rate (h^{-1})
WT	0.32 (±0.02)
$\Delta ldhA$	0.31 (±0.01)
$\Delta gap1\Delta ldhA$	0.28 (±0.01)
$gap1^{OEx}\Delta ldhA$	0.25 (±0.00)

2

Table 3. H_2 production (mol/mol glucose eq. catabolized from internal glycogen) and % of maximal theoretical yield for four strains of *Synechococcus* 7002: $\Delta gap1\Delta ldhA$, $gap1^{OEx}\Delta ldhA$, $\Delta ldhA$ and WT, under H_2 milking and non-milking conditions.

Strains	H₂/glu (mol/mol)		Yield (%)*	
	No milking (vol. 15 mL)[↑]	Milking	No milking (vol. 15 mL)[↑]	Milking
WT	0.16	0.73	1.32	6.06
$\Delta ldhA$	0.77	3.39	6.41	28.2
$\Delta gap1\Delta ldhA$	0.74	6.39	6.16	53.3
$gap1^{OEx}\Delta ldhA$	0.37	2.66	3.13	22.2

[↑]3-day average

*Yield (%) was calculated using $\dfrac{moles\ H_2}{mole\ Glucose\ eq\ *12} * 100$

3

Broader context:

An economic assessment of using photosynthetically generated biomass to produce H_2 through anaerobic digestion (fermentation) is directly determined by the product of the process efficiencies for the steps: (photosynthesis à biomass) x (biomass catabolism à fermentable substrate) x (substrate fermentation à H_2). Historically, the last step to H_2 has been restricted to low conversion yields and slow timescales. Herein, we demonstrate that metabolic engineering of cyanobacteria can improve both the efficiency of photosynthetic accumulation of glycogen (step 1) and significantly increase its net conversion by auto-fermentation to H_2 (step 3). This eliminates the second step altogether by directly making and using the fermentable substrate in the same microbe, while preserving cell viability for repetitive process cycling.